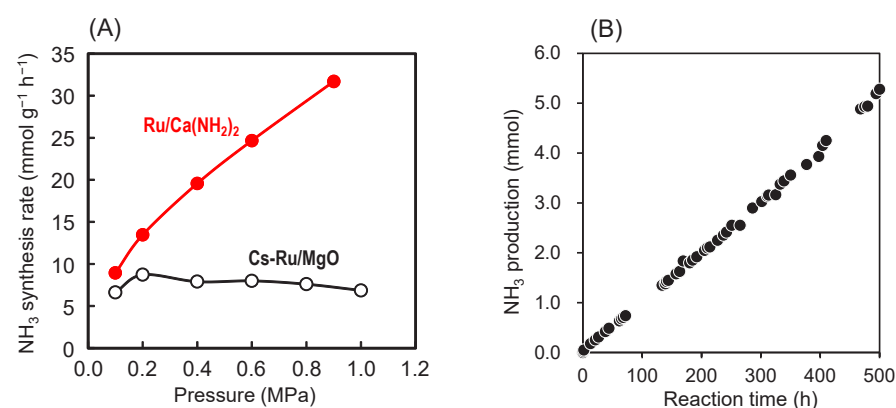


## Ammonia Synthesis over Self-Organized Flat Ru Nanoparticles on Calcium Amide

Ammonia ( $\text{NH}_3$ ) is an important chemical as a precursor for nitrogen fertilizers and has been expected to be used as a hydrogen (energy) carrier. Here, we report that flat-shaped ruthenium (Ru) nanoparticles with a narrow distribution ( $2.1 \pm 1.0$  nm) on calcium amide ( $\text{Ca}(\text{NH}_2)_2$ ) exhibit high catalytic performance far exceeding that of the conventional Ru-based catalysts. The results of X-ray absorption fine structure (XAFS) and high-angle annular dark field scanning transmission electron microscopy (HAADF-STEM) revealed that Ru nanoparticles are self-organized on the surface of  $\text{Ca}(\text{NH}_2)_2$  by strong Ru–N interaction during  $\text{NH}_3$  synthesis. The high catalytic performance is due to the formation of high-density flat-shaped Ru nanoparticles and the high electron donor ability of the support material.

The efficient synthesis of  $\text{NH}_3$  under low pressure and low temperature conditions is required because  $\text{NH}_3$  has attracted much attention as a material for storing hydrogen and also as an important precursor of nitrogen fertilizers, such as urea, which is one of the most widely-used agricultural chemicals in the world. The difficulty of synthesizing  $\text{NH}_3$  at low temperature comes from the very high dissociation energy of  $\text{N} \equiv \text{N}$  triple bonds. Although Ru-based catalysts are one of the most efficient  $\text{NH}_3$  synthesis catalysts, the catalytic activity is retarded by strong hydrogen adsorption onto the surface of Ru particles (hydrogen poisoning) [1]. To overcome this drawback of Ru, our group recently discovered a new catalyst, Ru-loaded  $12\text{CaO} \cdot 7\text{Al}_2\text{O}_3$  (C12A7) electride<sup>1</sup> (abbreviated as Ru/C12A7:e<sup>-</sup>) and Ru-loaded  $\text{Ca}_2\text{N}$  electride<sup>2</sup> (abbreviated as Ru/ $\text{Ca}_2\text{N}$ :e<sup>-</sup>), for  $\text{NH}_3$  synthesis, which effectively reduce the energy barrier for  $\text{N} \equiv \text{N}$  dissociation and suppress the hydrogen poisoning of Ru [2, 3]. However, there remain several obstacles to be resolved for practical application of a Ru-loaded electride. The disadvantage of C12A7:e<sup>-</sup> and  $\text{Ca}_2\text{N}$ :e<sup>-</sup> is their very small surface area (ca.  $1\text{--}3 \text{ m}^2 \text{ g}^{-1}$ ), which increases the size (20–30 nm) of deposited Ru particles and limits the catalytic performance of Ru-loaded electride. The optimum Ru particle size has been theoretically and experimentally demonstrated to be in the range 1.8–3.5 nm because the maximum number of surface step sites (B5-type site) is found in this range



**Figure 1:** (A)  $\text{NH}_3$  synthesis rate at 340°C over Ru(10%)/ $\text{Ca}(\text{NH}_2)_2$  and Cs-Ru(10%)/MgO as a function of reaction pressure. (B) Reaction time profile for  $\text{NH}_3$  synthesis over Ru(10%)/ $\text{Ca}(\text{NH}_2)_2$  at 200°C and 0.1 MPa. Total  $\text{NH}_3$  production reached 5.28 mmol after 500 h of reaction, which is more than ca. 4.2 times that produced due to the decomposition of  $\text{Ca}(\text{NH}_2)_2$  (0.09 g, 1.25 mmol). Reaction conditions: catalyst weight, 0.1 g; synthesis gas,  $\text{H}_2/\text{N}_2 = 3$ ; flow rate, 60  $\text{mL min}^{-1}$ .

[4]. A current challenge is how to realize a highly active catalyst for  $\text{NH}_3$  synthesis under mild conditions on the basis of this principle.

Recently, we reported a new high-performance catalyst for low-temperature  $\text{NH}_3$  synthesis that consists of  $\text{Ca}(\text{NH}_2)_2$  and Ru nanoparticles (Ru/ $\text{Ca}(\text{NH}_2)_2$ ) [5]. This catalyst has four notable advantages.

(i) The catalytic activity of Ru/ $\text{Ca}(\text{NH}_2)_2$  is an order of magnitude higher than that of the best catalyst reported to date (Cs promoted Ru/MgO catalyst) in terms of yield and turnover frequency (TOF)<sup>3</sup>. The kinetic data for Ru/ $\text{Ca}(\text{NH}_2)_2$  are similar to those of Ru/C12A7:e<sup>-</sup> and Ru/ $\text{Ca}_2\text{N}$ :e<sup>-</sup>, distinct from those of Cs-Ru/MgO.

(ii) The activity of Ru/ $\text{Ca}(\text{NH}_2)_2$  is not retarded by hydrogen poisoning. Figure 1A shows that the difference in  $\text{NH}_3$  synthesis rates over Ru/ $\text{Ca}(\text{NH}_2)_2$  and Cs-Ru/MgO increases significantly with the reaction pressure; distinct hydrogen poisoning is observed for Cs-Ru/MgO but not for Ru/ $\text{Ca}(\text{NH}_2)_2$ .

(iii) Ru/ $\text{Ca}(\text{NH}_2)_2$  also enables continuous  $\text{NH}_3$  production, even at 200°C under ambient pressure. (Fig. 1B)

(iv) Flat-shaped Ru nanoparticles are self-organized on  $\text{Ca}(\text{NH}_2)_2$  by a strong metal–support interaction between Ru and the  $\text{Ca}(\text{NH}_2)_2$  support. The strong metal–support interaction was demonstrated by XAFS analysis and HAADF-STEM observations.

Fourier transforms (FTs) of the  $k^2$ -weighted extended X-ray absorption fine structure (EXAFS) spectra for

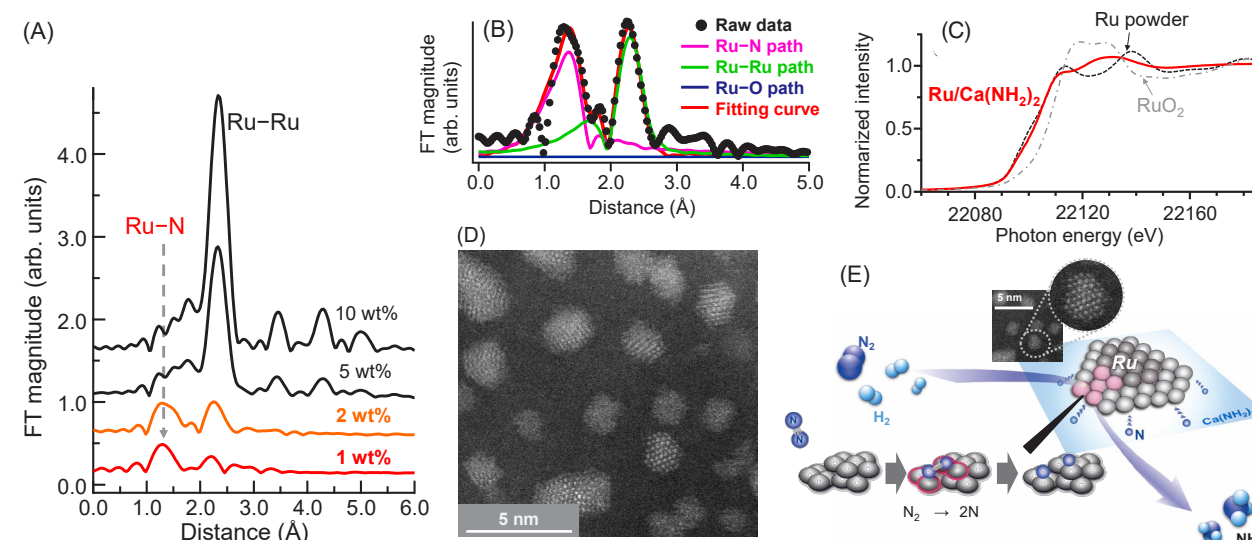


**Figure 2:** (A) FTs of the  $k^2$ -weighted EXAFS oscillations for various amounts of Ru-loaded  $\text{Ca}(\text{NH}_2)_2$  after  $\text{NH}_3$  synthesis. (Note these spectra are not corrected for phase shift.) (B) FT of Ru(2%)/ $\text{Ca}(\text{NH}_2)_2$  after  $\text{NH}_3$  synthesis (filled circles) and fitting curve for Ru–N, Ru–Ru, and Ru–O interactions. (C) Ru K-edge XANES spectra for Ru powder,  $\text{RuO}_2$ , and Ru(2%)/ $\text{Ca}(\text{NH}_2)_2$  after  $\text{NH}_3$  synthesis. (D) HAADF (High-Angle Annular Dark Field)-STEM image of Ru(10%)/ $\text{Ca}(\text{NH}_2)_2$  after  $\text{NH}_3$  synthesis. (E) Schematic illustration of  $\text{NH}_3$  synthesis over Ru/ $\text{Ca}(\text{NH}_2)_2$ .

Ru/ $\text{Ca}(\text{NH}_2)_2$  with various amounts of Ru-loading after  $\text{NH}_3$  synthesis are shown in Fig. 2A. A major peak is located at 2.3 Å, which corresponds to the Ru–Ru bond. Another peak was also observed at 1.3 Å for the 1 and 2 wt% Ru samples. We carefully tried fitting these data with Ru–O including an amorphous  $\text{RuO}_2$  model, Ru–N and Ru–Ru paths and successfully obtained a reasonable result with the Ru–N species model and Ru–Ru (R factor = 0.04057). In addition, the X-ray absorption near-edge structure (XANES) spectrum of Ru 2 wt% loaded sample shows a metallic state (Fig. 2B, C). If the oxidized species are present on the Ru surface, the absorption edge will shift to the higher energy region. Therefore, we conclude that the peak is not due to Ru-oxide species but to the Ru–N bond.

HAADF-STEM observations revealed that the flat-shaped Ru nanoparticles with a narrow distribution ( $2.1 \pm 1.0$  nm) are self-organized on  $\text{Ca}(\text{NH}_2)_2$  (Fig. 2D). The high Ru dispersion on Ru/ $\text{Ca}(\text{NH}_2)_2$  is attributed to strong interaction between Ru atoms and the N atoms of  $\text{Ca}(\text{NH}_2)_2$  on the basis of the XAFS results. Such a strong interaction prevents the aggregation of Ru particles during  $\text{NH}_3$  synthesis. To summarize these results, a schematic illustration of  $\text{NH}_3$  synthesis over Ru/ $\text{Ca}(\text{NH}_2)_2$  is shown in Figure 2E.

We also investigated the effect of promoting the catalytic activity of Ru/ $\text{Ca}(\text{NH}_2)_2$ . The results of nitrogen isotopic exchange reaction indicate that Ru/ $\text{Ca}(\text{NH}_2)_2$  catalyst facilitates the  $\text{N}_2$  cleavage, meaning that  $\text{Ca}(\text{NH}_2)_2$  also has high electron-donating ability to Ru [5]. However, no species with strong electron donating power are present for stoichiometric  $\text{Ca}(\text{NH}_2)_2$ . A plausible explanation for strong electron donation on Ru/ $\text{Ca}(\text{NH}_2)_2$  is the formation of hydride species ( $\text{H}^-$ ) at the Ru–support interfaces. Reversible exchange between hydride ions and electrons occurs at the Ru–support interfaces ( $\text{H}^0 +$

$\text{e}^- \leftrightarrow \text{H}^-$ ). A plausible route for the generation of such  $\text{H}^-$  during the reaction is via an F center with a low work function at the interface,  $\text{e}^-$  (F center) +  $\text{H}^0 \rightarrow \text{H}^-$ , resulting from the formation of  $\text{NH}_2^-$  vacancy and subsequent electron trapping at the vacancy site. Further efforts to examine this possible route are under way.

### NOTES

1) The chemical formula of a unit cell is expressed as  $[\text{C}_{24}\text{Al}_{28}\text{O}_{64}]^{4+}(\text{e}^-)_4$ . The former cation part is a positively charged lattice framework that possesses 12 sub-nanometer-sized cages with an inner free space (ca. 0.4 nm) in which electrons serve as anions.

2) A two-dimensional electride with a low work function (2.6 eV), in which anionic electrons are confined between the  $[\text{Ca}_2\text{N}]^+$  layers.

3) TOF is defined as the number of product molecules formed per surface site per second.

### REFERENCES

- S. E. Siporin and R. J. Davis, *J. Catal.* **225**, 359 (2004).
- M. Kitano, Y. Inoue, Y. Yamazaki, F. Hayashi, S. Kanbara, S. Matsuishi, T. Yokoyama, S. W. Kim, M. Hara and H. Hosono, *Nat. Chem.* **4**, 934 (2012).
- M. Kitano, Y. Inoue, H. Ishikawa, K. Yamagata, T. Nakao, T. Tada, S. Matsuishi, T. Yokoyama, M. Hara and H. Hosono, *Chem. Sci.* **7**, 4036 (2016).
- K. Honkala, A. Hellman, I. N. Remediakis, A. Logadottir, A. Carlsson, S. Dahl, C. H. Christensen and J. K. Nørskov, *Science* **307**, 555 (2005).
- Y. Inoue, M. Kitano, K. Kishida, H. Abe, Y. Niwa, M. Sasase, Y. Fujita, H. Ishikawa, T. Yokoyama, M. Hara and H. Hosono, *ACS Catal.* **6**, 7577 (2016).

### BEAMLINE

BL-NW10A

Y. Inoue<sup>1,†</sup>, M. Kitano<sup>1</sup>, H. Abe<sup>2,3</sup>, Y. Niwa<sup>2</sup>, T. Yokoyama<sup>1</sup>, M. Hara<sup>1,3</sup> and H. Hosono<sup>1,3</sup> (Tokyo Inst. of Tech., <sup>2</sup>KEK-PF, <sup>3</sup>ACCEL-JST, <sup>†</sup>Tokyo Metropolitan Univ. (Present address))